UCRL-JRNL-237329

LAWRENCE
LIVERMORE
NATIONAL
LABORATORY

A stable finite difference method for the elastic wave equation on complex geometries with free surfaces

D. Appelo, N. A. Petersson

December 18, 2007

Communications in Computational Physics

A stable finite difference method for the elastic wave equation on complex geometries with free surfaces

Daniel Appelö[1,*] and N. Anders Petersson[1]

[1] *Center for Applied and Scientific Computing, Lawrence Livermore National Laboratory, Livermore, Ca 94551, USA.*

Abstract.

AMS subject classifications: 65M06, 74B05, 86A15

Key words: elastic wave equation; curvilinear grids ; finite differences; stability; energy estimate; seismic wave propagation

1 Introduction

The isotropic elastic wave equation governs the propagation of seismic waves caused by earthquakes and other seismic events. It also governs the propagation of waves in solid material structures and devices, such as gas pipes, wave guides, railroad rails and disc brakes. In the vast majority of wave propagation problems arising in seismology and solid mechanics there are free surfaces. These free surfaces have, in general, complicated shapes and are rarely flat.

Another feature, characterizing problems arising in these areas, is the strong heterogeneity of the media, in which the problems are posed. For example, on the characteristic length scales of seismological problems, the geological structures of the earth can be considered piecewise constant, leading to models where the values of the elastic properties are also piecewise constant. Large spatial contrasts are also found in solid mechanics devices composed of different materials welded together.

The presence of curved free surfaces, together with the typical strong material heterogeneity, makes the design of stable, efficient and accurate numerical methods for the elastic wave equation challenging. Today, many different classes of numerical methods are used for the simulation of elastic waves. Early on, most of the methods were based on finite difference approximations of space and time derivatives of the equations in second order differential form (displacement formulation), see for example [1,2]. The main problem with these early discretizations were their inability to approximate free surface

*Corresponding author. *Email addresses:* appelo@kth.se (D. Appelö), andersp@llnl.gov (N. A. Petersson)

boundary conditions in a stable and fully explicit manner, see e.g. [10, 11, 18, 20]. The instabilities of these early methods were especially bad for problems with materials with high ratios between the P-wave (C_p) and S-wave (C_s) velocities.

For rectangular domains, a stable and explicit discretization of the free surface boundary conditions is presented in the paper [17] by Nilsson et al. In summary, they introduce a discretization, that use boundary-modified difference operators for the mixed derivatives in the governing equations. Nilsson et al. show that the method is second order accurate for problems with smoothly varying material properties and stable under standard CFL constraints, for *arbitrarily* varying material properties.

In this paper we generalize the results of Nilsson et al. to curvilinear coordinate systems, allowing for simulations on non-rectangular domains. Using summation by parts techniques, we show that there exists a corresponding stable discretization of the free surface boundary condition on curvilinear grids. We also prove that the discretization is stable and energy conserving both in semi-discrete and fully discrete form. As for the Cartesian method in, [17], the stability and conservation results holds for *arbitrarily varying material properties*. By numerical experiments it is established that the method is second order accurate.

The strengths of the proposed method are its ease of implementation, its (relative to low order unstructured grid methods) efficiency, its geometric flexibility, and, most importantly, its "bullet-proof" stability. On the downside, the main drawback of the suggested method is that it is only second order accurate. For wave propagation problems with smoothly varying material properties, it has been known for a long time [14] that low (2nd) order finite difference methods are less efficient than higher (4th or more) order finite difference methods. When the material properties are only piecewise smooth (as e.g. in seismology), the difference in efficiency between high and low order accurate finite difference methods is not as pronounced, see e.g. [4, 9]. For such problems the formal order of accuracy (for both high and low order methods) is reduced to one, but as has been shown in [4], the higher order methods produce more accurate results. Although we believe that the present method is reasonably competitive for strongly heterogeneous materials, it would be of great interest to derive a similarly "bullet-proof" fourth or higher order accurate method.

There are of course many other numerical methods capable of handling general geometries. Two recent finite difference methods, are the traction image method for curvilinear grids [21] and the embedded boundary method by Lombard et al. described in [15]. Especially the latter appear to be promising. Being an embedded boundary method it rids itself of the need to generate complicated meshes, a task that can be cumbersome for large scale problems that need to be run on large parallel computers. In comparison to the embedded boundary method of Lombard et al., the proposed method will work best for problems where most of the computations take place close to a surface (where an embedded boundary method have a large overhead) while the embedded boundary method work well for problems with large volume to surface ratio. Regarding the stability of the methods in [15, 21], there are no theoretical results described in the papers (in the latter stability is tested in a long-time simulation).

Other methods include the well-established spectral element method [7,13], the pseudospectral method [8] and the discontinuous Galerkin method [12]. For homogeneous materials these methods can, in principle, be made arbitrary accurate as the order n of the polynomial approximation increases. This property together with the geometrical flexibility of unstructured methods make spectral element and discontinuous Galerkin methods attractive for simulation of elastic waves in complex geometries. Unfortunately, the spectral radius of the discretized (with mesh size h) spatial operator scale as n^3/h for spectral elements and pseudospectral methods; and as n^2/h for discontinuous Galerkin methods. Thus, compared to finite difference methods whose spectral radius scale as n/h, the time stepping restrictions are rather severe (in practice this limits the order of approximation that can be used). As for finite difference methods, the formal order of these methods will be reduced to first order if material discontinuities are not aligned with element boundaries, see [6,9].

The rest of the paper is organized as follows: In §2 we state the governing equations and boundary conditions in Cartesian and curvilinear coordinates. We also describe a problem setup, which is used in §3 to illustrate the proposed numerical method. In §3 we introduce the proposed numerical method, and prove several results concerning its stability and conservation properties. Both the semi-discrete and fully discretized versions of the method are discussed. We also comment on how to extend the method to three dimensions. In §4 we give several numerical examples in two and three dimensions. We verify the order of the method and its discrete conservation properties for arbitrarily varying materials. Finally, in §5 we summarize and conclude.

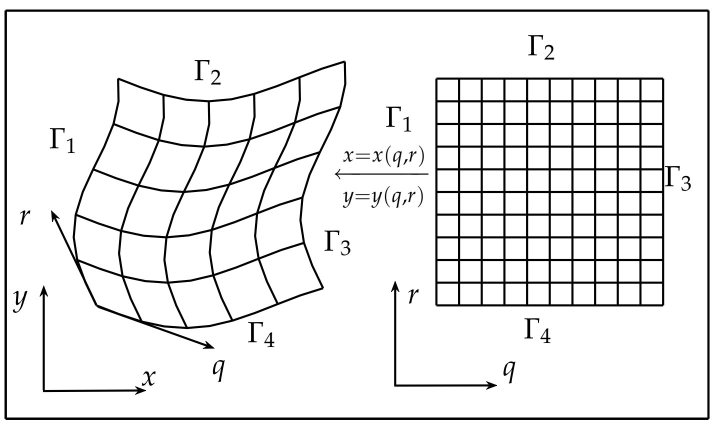

Figure 1: The Geometry. The free surface closest to $x=0$ is mapped onto to $q=0$ and the one closest to $y=0$ is mapped onto $r=0$.

2 The governing equations

Consider the propagation of elastic waves in a non-rectangular domain like the one depicted to the left in Figure 1. In a Cartesian coordinate system (the $x-y$ system to the left in Figure 1) the elastic wave equation, without external forcing, takes the form

$$\rho \frac{\partial^2 u}{\partial t^2} = \frac{\partial}{\partial x}\left((2\mu+\lambda)\frac{\partial}{\partial x}u + \lambda\frac{\partial}{\partial y}v\right) + \frac{\partial}{\partial y}\left(\mu\left(\frac{\partial}{\partial x}v + \frac{\partial}{\partial y}u\right)\right), \tag{2.1}$$

$$\rho \frac{\partial^2 v}{\partial t^2} = \frac{\partial}{\partial x}\left(\mu\left(\frac{\partial}{\partial x}v + \frac{\partial}{\partial y}u\right)\right) + \frac{\partial}{\partial y}\left(\lambda\frac{\partial}{\partial x}u + (2\mu+\lambda)\frac{\partial}{\partial y}v\right). \tag{2.2}$$

Here u and v are the displacements in the x and y directions. The Lamé parameters, $\mu = \mu(x,y)$ and $\lambda = \lambda(x,y)$ and the density $\rho = \rho(x,y)$, are restricted to be real valued positive functions, but are allowed to vary arbitrarily in space. The equations (2.1) - (2.2) are augmented by the initial data

$$u(x,y,0) = u_0(x,y), \quad v(x,y,0) = v_0(x,y),$$
$$\frac{\partial u(x,y,0)}{\partial t} = u_1(x,y), \quad \frac{\partial v(x,y,0)}{\partial t} = v_1(x,y).$$

To close the problem we need to specify boundary conditions and in this paper we consider three types of boundary conditions: free surface, Dirichlet and periodic boundary conditions. For simplicity, we first describe a case where only side Γ_1 (where $q=0$) is a free surface; later on (see §3.4) we describe how to discretize cases where two or more free surfaces are present.

On the free surface Γ_1 we impose the boundary conditions

$$\begin{bmatrix} (2\mu+\lambda)\frac{\partial u}{\partial x} + \lambda\frac{\partial v}{\partial y} & \mu(\frac{\partial v}{\partial x} + \frac{\partial u}{\partial y}) \\ \mu(\frac{\partial v}{\partial x} + \frac{\partial u}{\partial y}) & (2\mu+\lambda)\frac{\partial v}{\partial y} + \lambda\frac{\partial u}{\partial x} \end{bmatrix} \begin{bmatrix} n_x \\ n_y \end{bmatrix} = 0. \tag{2.3}$$

Here (n_x, n_y) is the inward normal of Γ_1. On the sides Γ_2, Γ_4 we impose periodic boundary conditions and on Γ_3 we impose homogeneous Dirichlet boundary conditions

$$u|_{\Gamma_3} = v|_{\Gamma_3} = 0. \tag{2.4}$$

2.1 The elastic wave equation in a curvilinear coordinate system

Before we discretize (2.1), (2.2) the governing equations and the boundary conditions are transformed to a curvilinear coordinate system that conforms with the boundaries of the domain, see Figure 1.

Assume that there is a one to one mapping

$$x(q,r), y(q,r), \quad (q,r) \in [0,1]^2,$$

from the unit square to the domain confined by $\Gamma_1,\Gamma_2,\Gamma_3,\Gamma_4$. By the chain rule we have the relations

$$\partial_x = q_x\partial_q + r_x\partial_r,\ \ \partial_y = q_y\partial_q + r_y\partial_r,\ \ \partial_q = x_q\partial_x + y_q\partial_y,\ \ \partial_r = x_r\partial_x + y_r\partial_y, \tag{2.5}$$

were q_x denotes $\frac{\partial q(x,y)}{\partial x}$ etc. and are referred to as metric derivatives or simply the metric. Inverting (2.5) we find the metric derivatives

$$\left[\begin{array}{cc} q_x & r_x \\ q_y & r_y \end{array}\right] = \frac{1}{J}\left[\begin{array}{cc} y_r & -y_q \\ -x_r & x_q \end{array}\right],$$

were $J = x_q y_r - x_r y_q$ is the Jacobian of the mapping.

Utilizing (2.5) the equations (2.1) and (2.2) are transformed into (for details see e.g [19])

$$\begin{aligned} J\rho\frac{\partial^2 u}{\partial t^2} = \frac{\partial}{\partial q}\Big[& Jq_x\left[(2\mu+\lambda)\left(q_x\partial_q + r_x\partial_r\right)u + \lambda\left(q_y\partial_q + r_y\partial_r\right)v\right] \\ & + Jq_y\left[\mu\left(\left(q_x\partial_q + r_x\partial_r\right)v + \left(q_y\partial_q + r_y\partial_r\right)u\right)\right]\Big] \\ & + \frac{\partial}{\partial r}\Big[Jr_x\left[(2\mu+\lambda)\left(q_x\partial_q + r_x\partial_r\right)u + \lambda\left(q_y\partial_q + r_y\partial_r\right)v\right] \\ & \qquad + Jr_y\left[\mu\left(\left(q_x\partial_q + r_x\partial_r\right)v + \left(q_y\partial_q + r_y\partial_r\right)u\right)\right]\Big], \end{aligned} \tag{2.6}$$

$$\begin{aligned} J\rho\frac{\partial^2 v}{\partial t^2} = \frac{\partial}{\partial q}\Big[& Jq_x\left[\mu\left(\left(q_x\partial_q + r_x\partial_r\right)v + \left(q_y\partial_q + r_y\partial_r\right)u\right)\right] \\ & + Jq_y\left[(2\mu+\lambda)\left(q_y\partial_q + r_y\partial_r\right)v + \lambda\left(q_x\partial_q + r_x\partial_r\right)u\right]\Big] \\ & + \frac{\partial}{\partial r}\Big[Jr_x\left[\mu\left(\left(q_x\partial_q + r_x\partial_r\right)v + \left(q_y\partial_q + r_y\partial_r\right)u\right)\right] \\ & \qquad + Jr_y\left[(2\mu+\lambda)\left(q_y\partial_q + r_y\partial_r\right)v + \lambda\left(q_x\partial_q + r_x\partial_r\right)u\right]\Big]. \end{aligned} \tag{2.7}$$

Similarly, the free surface boundary conditions are transformed into

$$\bar{q}_x\left[(2\mu+\lambda)(q_x u_q + r_x u_r) + \lambda(q_y v_q + r_y v_r)\right] + \bar{q}_y\mu((q_x v_q + r_x v_r) + (q_y u_q + r_y u_r)) = 0, \tag{2.8}$$

$$\bar{q}_x\mu((q_x v_q + r_x v_r) + (q_y u_q + r_y u_r)) + \bar{q}_y\left[(2\mu+\lambda)(q_x v_q + r_x v_r) + \lambda(q_y u_q + r_y u_r)\right] = 0. \tag{2.9}$$

Note that the normal is now represented by the normalized metric

$$\bar{q}_x = \frac{q_x}{\sqrt{q_x^2 + q_y^2}},\ \ \bar{q}_y = \frac{q_y}{\sqrt{q_x^2 + q_y^2}}.$$

We now proceed with the discretization of equations (2.6)- (2.7) and boundary conditions (2.8)- (2.9).

3 A self -adjoint discretization of the elastic wave equation on a curvilinear grid

To approximate (2.6) and (2.7) we cover the unit square with the grid

$$q_i = (i-1)h_q,\ \ i=0,\dots,N_q,\ \ h_q = 1/(N_q-1),$$
$$r_j = (j-1)h_r,\ \ j=0,\dots,N_r+1,\ \ h_r = 1/(N_r-1).$$

Here the grid indexes $(i,j)\in[1,N_q-1]\times[1,N_r]$ belong to interior points where (2.1), (2.2) are approximated and the rest belong to points that are assigned by enforcing the boundary conditions. On this grid we introduce the real valued grid functions $[u_{i,j},v_{i,j}] = [u(q_i,r_j,t),v(q_i,r_j,t)]$ and the standard the difference operators

$$D_+^q u_{i,j} = \frac{u_{i+1,j}-u_{i,j}}{h_q},\ \ D_-^q u_{i,j} = D_+^q u_{i-1,j},$$
$$D_+^r u_{i,j} = \frac{u_{i,j+1}-u_{i,j}}{h_r},\ \ D_-^r u_{i,j} = D_+^r u_{i,j-1},$$
$$D_0^q u_{i,j} = \frac{1}{2}(D_+^q u_{i,j}+D_-^q u_{i,j}),\ \ D_0^r u_{i,j} = \frac{1}{2}(D_+^r u_{i,j}+D_-^r u_{i,j}),$$

as well as the boundary modified operator

$$\widetilde{D_0^q} u_{i,j} = \begin{cases} D_+^q u_{i,j}, & i=1, \\ D_0^q u_{i,j}, & i\geq 2. \end{cases}$$

We also introduce the averaging operators

$$E_{1/2}^q(\sigma_{i,j}) = \frac{1}{2}(\sigma_{i+1,j}+\sigma_{i,j}),\ \ E_{1/2}^r(\sigma_{i,j}) = \frac{1}{2}(\sigma_{i,j+1}+\sigma_{i,j}).$$

3.1 The spatial discretization

We approximate the spatial operators in equations (2.6) and (2.7) by (the grid indexes have been suppressed to increase the readability)

$$\begin{aligned} J\rho\frac{\partial^2 u}{\partial t^2} &= D_-^q E_{1/2}^q(Jq_xq_x(2\mu+\lambda))D_+^q u + \widetilde{D_0^q}(Jq_xr_x(2\mu+\lambda))D_0^r u + D_-^q E_{1/2}^q(Jq_xq_y\lambda)D_+^q v \\ &+ \widetilde{D_0^q}(Jq_xr_y\lambda)D_0^r v + D_-^q E_{1/2}^q(Jq_yq_x\mu)D_+^q v + \widetilde{D_0^q}(Jq_yr_x\mu)D_0^r v + D_-^q E_{1/2}^q(Jq_yq_y\mu)D_+^q u \\ &+ \widetilde{D_0^q}(Jq_yr_y\mu)D_0^r u + D_0^r(Jr_xq_x(2\mu+\lambda))\widetilde{D_0^q}u + D_-^r E_{1/2}^r(Jr_xr_x(2\mu+\lambda))D_+^r u \\ &+ D_0^r(Jr_xq_y\lambda)\widetilde{D_0^q}v + D_-^r E_{1/2}^r(Jr_xr_y\lambda)D_+^r v + D_0^r(Jr_yq_x\mu)\widetilde{D_0^q}v + D_-^r E_{1/2}^r(Jr_yr_x\mu)D_+^r v \\ &+ D_0^r(Jr_yq_y\mu)\widetilde{D_0^q}u + D_-^r E_{1/2}^r(Jr_yr_y\mu)D_+^r u \equiv L^{(u)}(u,v). \quad (3.1) \end{aligned}$$

$$
\begin{aligned}
J\rho\frac{\partial^2 v}{\partial t^2} = {} & D_-^q E_{1/2}^q(Jq_xq_x\mu)D_+^q v + \widetilde{D_0^q}(Jq_xr_x\mu)D_0^r v + D_-^q E_{1/2}^q(Jq_xq_y\mu)D_+^q u + \widetilde{D_0^q}(Jq_xr_y\mu)D_0^r u \\
& + D_-^q E_{1/2}^q(Jq_yq_x\lambda)D_+^q u + \widetilde{D_0^q}(Jq_yr_x\lambda)D_0^r u + D_-^q E_{1/2}^q(Jq_yq_y(2\mu+\lambda))D_+^q v \\
& + \widetilde{D_0^q}(Jq_yr_y(2\mu+\lambda))D_0^r v + D_0^r(Jr_xq_x\mu)\widetilde{D_0^q}v + D_-^r E_{1/2}^r(Jr_xr_x\mu)D_+^r v + D_0^r(Jr_xq_y\mu)\widetilde{D_0^q}u \\
& + D_-^r E_{1/2}^r(Jr_xr_y\mu)D_+^r u + D_0^r(Jr_yq_x\lambda)\widetilde{D_0^q}u + D_-^r E_{1/2}^r(Jr_yr_x\lambda)D_+^r u + D_0^r(Jr_yq_y(2\mu+\lambda))\widetilde{D_0^q}v \\
& + D_-^r E_{1/2}^r(Jr_yr_y(2\mu+\lambda))D_+^r v \equiv L^{(v)}(u,v), \quad (3.2)
\end{aligned}
$$

in the grid points $(q_i,r_j),(i,j)\in[1,N_q-1]\times[1,N_r]$. The discrete boundary conditions corresponding to (2.4) are

$$
\left.\begin{aligned} u_{N_q,j} &= 0 \\ v_{N_q,j} &= 0 \end{aligned}\right\} \quad \text{for } j=1,\dots,N_r, \tag{3.3}
$$

and the periodic boundary conditions are $w_{i,j}=w_{i,j+N_r}, w=u,v$ and can be used to specify

$$
\left.\begin{aligned} u_{i,0} &= u_{i,N_r}, \quad u_{i,N_r+1} = u_{i,1}, \\ v_{i,0} &= v_{i,N_r}, \quad v_{i,N_r+1} = v_{i,1}, \end{aligned}\right\} \quad \text{for } i=0,\dots,N_q, \tag{3.4}
$$

Finally, as we are about to show, stable second order accurate approximations of the free surface boundary conditions (2.8), (2.9) are given by

$$
\begin{aligned}
& \frac{1}{2}\left((Jq_xq_x(2\mu+\lambda))_{3/2,j}D_+^q u_{1,j} + (Jq_xq_x(2\mu+\lambda))_{1/2,j}D_+^q u_{0,j}\right) + (Jq_xr_x(2\mu+\lambda))_{1,j}D_0^r u_{1,j} \\
& \quad + \frac{1}{2}\left((Jq_xq_y\lambda)_{3/2,j}D_+^q v_{1,j} + (Jq_xq_y\lambda)_{1/2,j}D_+^q v_{0,j}\right) + (Jq_xr_y\lambda)_{1,j}D_0^r v_{1,j} \\
& \quad + \frac{1}{2}\left((Jq_yq_x\mu)_{3/2,j}D_+^q v_{1,j} + (Jq_yq_x\mu)_{1/2,j}D_+^q v_{0,j}\right) + (Jq_yr_x\mu)_{1,j}D_0^r v_{1,j} \\
& + \frac{1}{2}\left((Jq_yq_y\mu)_{3/2,j}D_+^q u_{1,j} + (Jq_yq_y\mu)_{1/2,j}D_+^q u_{0,j}\right) + (Jq_yr_y\mu)_{1,j}D_0^r u_{1,j} = 0, \quad \text{for } j=1,\dots,N_r,
\end{aligned} \tag{3.5}
$$

$$
\begin{aligned}
& \frac{1}{2}\left((Jq_xq_x\mu)_{3/2,j}D_+^q v_{1,j} + (Jq_xq_x\mu)_{1/2,j}D_+^q v_{0,j}\right) + \left((Jq_xr_x\mu)_{1,j}D_0^r v_{1,j}\right) \\
& \quad + \frac{1}{2}\left((Jq_xq_y\mu)_{3/2,j}D_+^q u_{1,j} + (Jq_xq_y\mu)_{1/2,j}D_+^q u_{0,j}\right) + \left((Jq_xr_y\mu)_{1,j}D_0^r u_{1,j}\right) \\
& + \frac{1}{2}\left((Jq_yq_y(2\mu+\lambda))_{3/2,j}D_+^q v_{1,j} + (Jq_yq_y(2\mu+\lambda))_{1/2,j}D_+^q v_{0,j}\right) + \left((Jq_yr_y(2\mu+\lambda))_{1,j}D_0^r v_{1,j}\right) \\
& + \frac{1}{2}\left((Jq_yq_x\lambda)_{3/2,j}D_+^q u_{1,j} + (Jq_yq_x\lambda)_{1/2,j}D_+^q u_{0,j}\right) + \left((Jq_yr_x\lambda)_{1,j}D_0^r u_{1,j}\right) = 0, \quad \text{for } j=1,\dots,N_r.
\end{aligned} \tag{3.6}
$$

Remark 1. The key ingredient in obtaining a stable self-adjoint *explicit* discretization is to use the one-sided operator $\widetilde{D_0^q}$ for the approximation of the normal derivative in the $\partial_q\partial_r$ and $\partial_r\partial_q$ cross derivatives. At first, it might appear that by using the one-sided operator the order of the method would be reduced. However, as was theoretically shown in [17] (for a Cartesian discretization) and will be shown by numerical experiments below the discretization produce second order accurate solutions.

Remark 2. The above discretization does not depend on how the metric derivatives are computed. If the mapping is known explicitly they can be computed analytically, if not they can be computed numerically. In all numerical examples presented in this paper the metric derivatives are computed numerically using second order accurate finite difference approximations.

3.2 Some lemmata about the discretization

In this subsection we state and prove the main properties of the discretization. We begin by defining a suitable discrete inner product. Let w and u be real valued grid functions and $(w,u)_h$ be the discrete inner product

$$(w,u)_h = h_q h_r \sum_{j=1}^{N_r} \left(\frac{1}{2} w_{1,j} u_{1,j} + \sum_{i=2}^{N_q} w_{i,j} u_{i,j} \right),$$

with corresponding norm $\|w\|_h^2 = (w,w)_h$. For the present discretization we have.

Lemma 1 (Self adjointness of the spatial discretization). For all real-valued grid functions (u^0,v^0), (u^1,v^1) satisfying the discrete boundary conditions (3.3), (3.4), (3.5), (3.6), the spatial operator $(L^{(u)},L^{(v)})$ is self-adjoint, i.e.

$$(u^0,L^{(u)}(u^1,v^1))_h + (v^0,L^{(v)}(u^1,v^1))_h = (u^1,L^{(u)}(u^0,v^0))_h + (v^1,L^{(v)}(u^0,v^0))_h. \tag{3.7}$$

Proof. Our first step is to show that $(u^0,L^{(u)}(u^1,v^1))_h = (u^1,L^{(u)}(u^0,v^0))_h$, we will do this by transferring "half" of the difference approximations (to the right in the inner products) onto the solitary u^0 or u^1 to the left in the inner products. To do this we use the following summation by part identities

$$\begin{aligned}
&(D_+^r w,u)_h + (w,D_-^r u)_h = 0,\\
&(D_0^r w,u)_h + (w,D_0^r u)_h = 0,\\
&(w,D_+^q u)_h + (D_-^q w,u)_h = -\frac{h_r}{2} \sum_{j=1}^{N_r-1} \left(w_{0,j} u_{1,j} + w_{1,j} u_{2,j} \right) + h_r \sum_{j=1}^{N_r} w_{N_q-1,j} u_{N_q,j},\\
&(w,\widetilde{D_0^q} u)_h + (\widetilde{D_0^q} w,u)_h = -h_r \sum_{j=1}^{N_r} w_{1,j} u_{1,j} + \frac{h_r}{2} \sum_{j=1}^{N_r} \left(w_{N_q,j} u_{N_q-1,j} + w_{N_q-1,j} u_{N_q,j} \right).
\end{aligned} \tag{3.8}$$

We illustrate the ideas of the proof on the first two terms the inner product $(u^0, L^{(u)}(u^1, v^1))_h$. Starting with the first $\partial_q\partial_q$ term, $D_-^q E_{1/2}^q (Jq_x q_x(2\mu+\lambda))D_+^q u$, we apply the above summation by parts identities and find

$$
\begin{aligned}
(u^0, D_-^q E_{1/2}^q (Jq_x q_x(2\mu+\lambda))D_+^q u^1) = &-(D_+^q u^0, E_{1/2}^q (Jq_x q_x(2\mu+\lambda))D_+^q u^1) \\
&\underbrace{+h_r \sum_{j=1}^{N_r} u^0_{N_q,j}(Jq_x q_x(2\mu+\lambda))_{N_q-1/2,j} D_+^q u^1_{N_q-1,j}}_{A_1} \\
&\underbrace{-\frac{h_r}{2}\sum_{j=1}^{N_r}\Big(u^0_{2,j}(Jq_x q_x(2\mu+\lambda))_{3/2,j} D_+^q u^1_{1,j} + u^0_{1,j}(Jq_x q_x(2\mu+\lambda))_{1/2,j} D_+^q u^1_{0,j}\Big)}_{B_1}.
\end{aligned}
$$

The homogeneous Dirichlet boundary condition on Γ_3 is $u^0_{N_q,j} = 0$ thus the term A_1 vanishes, leaving only the boundary contribution B_1. To get an expression for B_1 where $u^0_{1,j}$ multiplies the terms containing D_+^q (which is an approximation of the $q_x(2\mu+\lambda)u_q$ part of the boundary condition) we use the identity $u^0_{2,j} = u^0_{1,j} + h_q D_+^q u^0_{1,j}$ and obtain

$$
\begin{aligned}
B_1 = &\underbrace{-\frac{h_r}{2}\sum_{j=1}^{N_r} u^0_{1,j}\Big((Jq_x q_x(2\mu+\lambda))_{3/2,j} D_+^q u^1_{1,j} + (Jq_x q_x(2\mu+\lambda))_{1/2,j} D_+^q u^1_{0,j}\Big)}_{\mathfrak{B}_1(u^0,u^1,v^0,v^1)} \\
&\underbrace{-\frac{h_r h_q}{2}\sum_{j=1}^{N_r} D_+^q u^0_{1,j}(Jq_x q_x(2\mu+\lambda))_{3/2,j} D_+^q u^1_{1,j}}_{b_1}.
\end{aligned}
$$

The term b_1 is symmetric in u^0, u^1 and there is an identical contribution, canceling b_1, from the first term in $(u^1, L^{(u)}(u^0, v^0))_h$.

For the second term, $\widetilde{D_0^q}(Jq_x r_x(2\mu+\lambda))D_0^r u^1$, in $(u^0, L^{(u)}(u^1, v^1))_h$ the above identities are used again to obtain

$$
\begin{aligned}
(u^0, \widetilde{D_0^q}(Jq_x r_x(2\mu+\lambda))D_0^r u^1) = &-(\widetilde{D_0^q} u^0, (Jq_x r_x(2\mu+\lambda))D_0^r u^1) \\
&\underbrace{+\frac{h_r}{2}\sum_{j=1}^{N_r}\big(u^0_{N_q-1,j}(Jq_x r_x(2\mu+\lambda))_{N_q,j} D_0^r u^1_{N_q,j} + u^0_{N_q,j}(Jq_x r_x(2\mu+\lambda))_{N_q+1,j} D_0^r u^1_{N_q-1,j}\big)}_{A_2} \\
&\underbrace{-h_r\sum_{j=1}^{N_r} u^0_{1,j}\Big((Jq_x r_x(2\mu+\lambda))_{1,j} D_0^r u^1_{1,j}\Big)}_{\mathfrak{B}_2(u^0,u^1,v^0,v^1)}.
\end{aligned}
$$

We note that $u^1_{N_q,j}=0$ implies $D^r_0 u^1_{N_q,j}=0$ and thus the boundary term A_2 vanishes.

The six remaining of the first eight terms in $(u^0,L^{(u)}(u^1,v^1))_h$ gives the same type of contributions and the last eight terms will not give any boundary contributions because of the periodicity in the r direction.

Repeating the above steps for $(u^1,L^{(u)}(u^0,v^0))_h$ give the same kind of boundary terms (the arguments of $\mathfrak{B}_k$ are ordered differently, namely $\mathfrak{B}_k(u^1,u^0,v^1,v^0)$). From $(v^0,L^{(v)}(u^1,v^1))_h$ and $(v^1,L^{(v)}(u^0,v^0))_h$ there will also be boundary terms, which we denote $\mathfrak{C}_k(u^0,u^1,v^0,v^1)$ and $\mathfrak{C}_k(u^1,u^0,v^1,v^0)$ respectively. Subtracting the right hand side of the left hand side of equation (3.7) results in the equality

$$\begin{aligned}&(u^0,L^{(u)}(u^1,v^1))_h-(u^0,L^{(u)}(u^1,v^1))_h+(v^0,L^{(v)}(u^1,v^1))_h-(v^0,L^{(v)}(u^1,v^1))_h=\\&\sum_{k=1}^{8}\mathfrak{B}_k(u^0,u^1,v^0,v^1)-\sum_{k=1}^{8}\mathfrak{B}_k(u^1,u^0,v^1,v^0)+\sum_{k=1}^{8}\mathfrak{C}_k(u^0,u^1,v^0,v^1)-\sum_{k=1}^{8}\mathfrak{C}_k(u^1,u^0,v^1,v^0).\end{aligned}\tag{3.9}$$

The first term on the right hand of (3.9) side is

$$\begin{aligned}\sum_{k=1}^{8}\mathfrak{B}_k(u^0,u^1,v^0,v^1)=&-\sum_{j=1}^{N_r}u^0_{1,j}\Big[\frac{1}{2}\Big((Jq_xq_x(2\mu+\lambda))_{3/2,j}D^q_+u^1_{1,j}+(Jq_xq_x(2\mu+\lambda))_{1/2,j}D^q_+u^1_{0,j}\Big)\\&+(Jq_xr_x(2\mu+\lambda))_{1,j}D^r_0u^1_{1,j}+\frac{1}{2}\Big((Jq_xq_y\lambda)_{3/2,j}D^q_+v^1_{1,j}+(Jq_xq_y\lambda)_{1/2,j}D^q_+v^1_{0,j}\Big)\\&+(Jq_xr_y\lambda)_{1,j}D^r_0v^1_{1,j}+\frac{1}{2}\Big((Jq_yq_x\mu)_{3/2,j}D^q_+v^1_{1,j}+(Jq_yq_x\mu)_{1/2,j}D^q_+v^1_{0,j}\Big)\\&+(Jq_yr_x\mu)_{1,j}D^r_0v^1_{1,j}+\frac{1}{2}\Big((Jq_yq_y\mu)_{3/2,j}D^q_+u^1_{1,j}+(Jq_yq_y\mu)_{1/2,j}D^q_+u^1_{0,j}\Big)+(Jq_yr_y\mu)_{1,j}D^r_0u^1_{1,j}\Big].\end{aligned}\tag{3.10}$$

The factor within the square brackets multiplying $u^0_{1,j}$ is identical to the boundary condition (3.5) and therefore vanishes. The second term of (3.9) also vanishes due to (3.5) and, finally, the third and fourth terms vanishes due to the boundary condition (3.6). This finalizes the proof. $\square$

A direct consequence of lemma 1 is the following corollary.

Corollary 1 (Conservation of energy). All real-valued solutions (u,v) to the equations (3.1), (3.2) with boundary conditions (3.3), (3.4), (3.5) and (3.6), satisfy

$$\|\sqrt{J\rho}\,u_t\|_h^2+\|\sqrt{J\rho}\,v_t\|_h^2-(u,L^{(u)}(u,v))_h-(v,L^{(v)}(u,v))_h=C.\tag{3.11}$$

Here C is a constant depending only on the initial data.

Proof. Lemma 1 gives

$$\frac{1}{2}\frac{d}{dt}\left(\|\sqrt{J\rho}u_t\|_h^2+\|\sqrt{J\rho}v_t\|_h^2\right)=$$
$$\frac{1}{2}\left((u_t,L^{(u)}(u,v))_h+(v_t,L^{(v)}(u,v))_h+(u,L^{(u)}(u_t,v_t))_h+(v,L^{(v)}(u_t,v_t))_h\right)=$$
$$\frac{1}{2}\frac{d}{dt}\left((u,L^{(u)}(u,v))_h+(v,L^{(v)}(u,v))_h\right).$$

Integrating in time we arrive at (3.11). □

For the quantity in (3.11) to be an energy we need the following result.

Lemma 2 (Ellipticity). For all real-valued grid functions (u,v) satisfying the discrete boundary conditions (3.3), (3.4), (3.5), (3.6), the spatial operators $L^{(u)}(u,v)$ and $L^{(v)}(u,v)$ satisfy

$$-(u,L^{(u)}(u,v))_h-(v,L^{(v)}(u,v))_h=\mathcal{P}_1+\mathcal{P}_2+\mathcal{P}_3+\mathcal{P}_4, \tag{3.12}$$

with (the exact expressions can be found in appendix A)

$$\mathcal{P}_1\geq 0,\ \ \mathcal{P}_2\geq 0,\ \ \mathcal{P}_3\geq 0,\ \ \mathcal{P}_4\geq 0.$$

Proof. The equality (3.12) is derived by using the following summation by parts identities

$$(u,D_-^rE_{1/2}^r(\sigma)D_+^rv)_h=-\underbrace{(D_0^ru,D_0^rv)_h}_{t_1}-\underbrace{\frac{h_r^2}{4}(D_+^rD_-^ru,\sigma D_+^rD_-^rv)_h}_{t_2},$$

$$(u,D_-^qE_{1/2}^q(\sigma)D_+^qv)_h=-\underbrace{(D_0^qu,D_0^qv)_h}_{t_3}-\underbrace{\frac{h_q^2}{4}(D_+^qD_-^ru,\sigma D_+^qD_-^qv)_{hr}}_{t_4}$$
$$+h_r\sum_{j=1}^{N_r}\Big(-\frac{1}{2}\sigma_{1/2,j}u_{1,j}D_+^qv_{0,j}-\underbrace{\frac{1}{2}\sigma_{3/2,j}u_{2,j}D_+^qv_{1,j}}_{t_5}$$
$$+\underbrace{\frac{\sigma_{N_q,j}}{2}u_{N_q-1,j}D_+^qu_{N_q-1,j}}_{t_6}+\underbrace{\frac{\sigma_{N_q-1,j}}{2}u_{N_q,j}D_+^qu_{N_q-1,j}}_{t_7}\Big),$$

together with the identities (3.8). Here the inner product $(w,v)_{hr}$ is defined as

$$(w,u)_h=h_qh_r\sum_{j=1}^{N_r}\sum_{i=2}^{N_q}w_{i,j}u_{i,j}.$$

The corresponding norm is $\|w\|_{hr}^2=(w,w)_{hr}$.

To verify (3.12), terms of the type t_1 and t_3 are collected into $\mathcal{P}_1$ and terms of type t_2 and t_4 into $\mathcal{P}_2$. The t_7 and one part of the t_6 terms vanishes due to the homogeneous Dirichlet boundary conditions (3.3), the remaining contribution from the t_6 term goes into $\mathcal{P}_3$. Using $u_{2,j} = u_{1,j} + h_q D_+^q u_{1,j}$ on the t_5 term gives the contributions of $\mathcal{P}_4$. Collecting all the remaining boundary terms gives an expression identical to (3.10) (with $u^0 = u^1 = u$) and another term identical to the expression corresponding to (3.10) for the second free surface boundary condition (3.6). As the free surface boundary conditions are assumed to hold, the lemma is proved. $\square$

3.3 Temporal discretization

In time we discretize using second order accurate centered differences. The fully discrete equations are

$$\begin{aligned} u^{n+1} - 2u^n + u^{n-1} &= (\rho J)^{-1} k^2 L^{(u)}(u^n, v^n), \\ v^{n+1} - 2v^n + v^{n-1} &= (\rho J)^{-1} k^2 L^{(v)}(u^n, v^n). \end{aligned} \tag{3.13}$$

For the fully discrete equations it can be shown that the following lemma holds.

Lemma 3.1 (Discrete conservation of energy). *Let $(u,v)_{\rho J}$ be the weighted inner product defined by $(f, g/(\rho J))_{\rho J} = (f,g)_h$, and let $C_e(t_{n+1})$ be the discrete energy*

$$\begin{aligned} &C_e(t_{n+1}) = \\ &\|D_+^t u^n\|_{\rho J}^2 + \|D_+^t v^n\|_{\rho J}^2 - (u^{n+1}, (\rho J)^{-1} L^{(u)}(u^n, v^n))_{\rho J} - (v^{n+1}, (\rho J)^{-1} L^{(v)}(u^n, v^n))_{\rho J}. \end{aligned} \tag{3.14}$$

If $u^q, v^q, q = n-1, n, n+1$ are solutions to (3.13) and satisfy the discrete boundary conditions (3.3), (3.4), (3.5), (3.6) then

$$C_e(t_{n+1}) = C_e(t_n).$$

The proof of the lemma is the same as for the Cartesian discretization and can be found in [17] (theorem 3).

3.4 Corners where free surfaces meet

As was stated above, the key ingredient to obtain a stable and explicit discretization of the free surface at Γ_1 is to use the boundary modified difference operator $\widetilde{D_0^q}$ for the normal derivative in the cross derivative terms in the equation. For cases with more than one free surface we use difference operators that are modified at those other free surfaces as well. For example, when the boundary Γ_4 is changed into a free surface and the boundary Γ_2 is changed into a homogeneous Dirichlet boundary, the grid in r is changed to

$$r_j = (j-1)h_r, \;\; j = 0, \ldots, N_r, \;\; h_r = 1/(N_r - 1).$$

Now the grid indexes $(i,j)\in[1,N_q-1]\times[1,N_r-1]$ belong to interior points. Also, the discretization of the equations is changed by using the modified operator

$$\widetilde{D_0^r}u_{i,j}=\begin{cases} D_+^r u_{i,j}, & j=1, \\ D_0^r u_{i,j}, & j\geq 2, \end{cases}$$

instead of D_0^r. Now, at the point (q_1,r_1) we need to use the free surface boundary conditions on Γ_1 to get the values for $u_{0,1}$ and $v_{0,1}$ and the free surface boundary conditions on Γ_4 to get the values for $u_{1,0}$ and $v_{1,0}$. By repeating the steps in the proofs of the different lemmata it is easy to see that for the self-adjointness and conservation results to hold we have to modify the discretization of the boundary conditions at the corners. Not surprisingly, the correct modification consists of replacing D_0^r by $\widetilde{D_0^r}$ in (3.1) and (3.2) and replacing D_0^q by $\widetilde{D_0^q}$ in the free surface boundary condition discretization along Γ_4. These modifications, apart from being necessary for stability, are also good from an implementations point of view because all free surface boundaries can be updated independent of each other, keeping the method fully explicit.

When implementing the method in a practical computer code it is important to apply the boundary conditions in the correct order. Given the solution on the two previous time levels n and $n-1$ the steps to advance the solution to time level $n+1$ are the following:

1. Update all Dirichlet b.c.

2. Update all periodic b.c.

3. Update all free-surface b.c.

4. Use equation (3.13) to get the solution at t_{n+1}.

3.4.1 Extension to three dimensions

The extension of the scheme to three dimensions is straightforward. Given a one to one mapping $(x(q,r,s),y(q,r,s),z(q,r,s)),q,r,s\in[0,1]$, the three dimensional elastic wave equation can be formulated in conservative form in the curvilinear coordinate system. The resulting equations are discretized in the same way as (2.6)- (2.7). Again, if a boundary has free surface condition, then a modified difference operator is used for the normal derivative in the cross derivative term in the governing equation. As for the corner case above, at edges between free surfaces the modified difference operators for the *tangential derivatives in the free surface boundary conditions* are used. The same recipe is used for the tangential derivatives in the boundary conditions in three dimensions corners where three free surfaces meet.

Remark 3. It is straightforward (but tedious) to show that lemma 1, 2 and corollary 1 in §3.2 carry over directly to the three dimensional case.

4 Numerical examples

In this section we present numerical experiments with the numerical method described above. We start with two verification examples and proceed with four more application oriented examples, illustrating the versatility of the method.

4.1 Verification: Method of manufactured solution in two dimensions

N	maxerr u	maxerr v	$e_i/e_{i+1},u$	$e_i/e_{i+1},v$
80	0.16533	0.15609		
160	0.04245	0.03912	3.89	3.99
320	0.01071	0.00971	3.96	4.03
640	0.00269	0.00240	3.98	4.04

Table 1: Experimentally determined order of accuracy using the method of manufactured solution.

A powerful way to verify the correctness of the implementation of any numerical method is the method of manufactured solution. The method works as follows: postulate a smooth solution described by functions that are easy to differentiate. In this example we choose

$$u = \sin(6.2(x-1.3t))\sin(6.2y), \tag{4.1}$$

$$v = \sin(6.2(x-1.2t))\sin(6.2y). \tag{4.2}$$

Insert the postulated solution into the governing equations and the boundary conditions to determine the external forcing that would give the desired solution (for example, if the equation was $u_t+u_x=f$, then we would set $f=6.2(1-1.3)\cos(6.2(x-1.3t))\sin(6.2y)$ in order to manufacture the solution (4.1)).

The computational domain we considerer is defined by the mapping

$$x = q+0.05\sin(\pi(r-0.5)), \;\; y = r+0.05\sin(\pi(q-0.5)),$$
$$(q,r)\in[0,1]^2.$$

The surfaces corresponding to $q=0$ and $r=0$ are free and the surfaces $q=1$ and $r=1$ are clamped, i.e. Dirichlet boundary conditions are enforced. We choose the Lamé parameters to be $\lambda=\mu=1$ and advanced the solution up to time $\pi/5$ with a time step $k=0.1h$, were, $h_r=h_q=h=\pi/N, N=80,160,320,640$. At the final time the maximum error is computed and tabulated in Table 1. From the results we conjecture that the method is second order accurate.

4.2 Verification: Conservation of discrete energy in three dimensions

The fact that the scheme conserves a discrete energy can be used as another tool to to verify the correctness of the code. The idea is to use random (but physically valid $\rho,\lambda,\mu>$

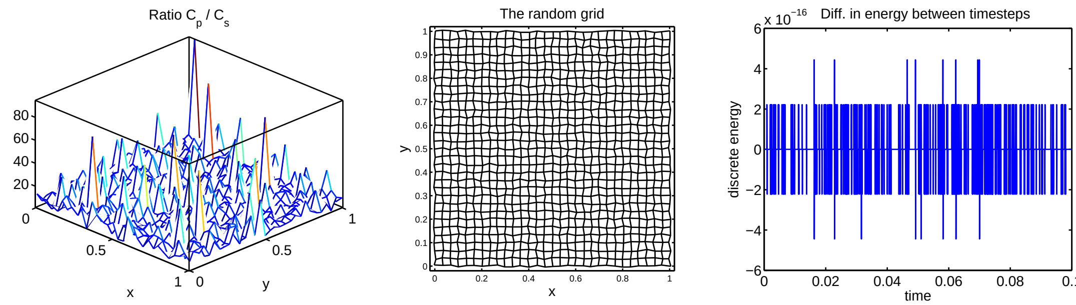

Figure 2: To the left: Ratio of the randomly chosen P and S - wave velocities on the free surface $s=0$. In the middle: The grid on the free surface $s=0$. The grid is made up of a regular Cartesian grid whose grid-points has been randomly perturbed. To the right: The difference in the (3D version) discrete energy (3.14) of subsequent time steps. The discrete energy is conserved to machine precision.

0) data for the initial values, the material parameters and for the grid (we require $J>0$).

The grid is constructed by first discretizing the 3D unit cube with a grid spacing of $1/40$, then the x,y,z coordinates of all regular grid points are perturbed by a uniformly distributed random variable taking values in $[-0.005, 0.005]$. A plot of the first vertical grid plane (corresponding to $s=0$) projected onto the x-y plane can be found in Figure 2. The Lamé parameters are given by

$$\lambda(x,y,z)=1+R_{10000}, \quad \mu(x,y,z)=1+R_{100},$$

where R_p is a uniformly distributed random variable taking values in $[0,p]$. A plot of the point-wise ratio between C_p and C_s can be found in Figure 2. The initial data is prescribed as uniformly distributed random variables, with a magnitude chosen such that the initial discrete energy is of order one. Free-surface boundary conditions are imposed on the top and bottom of the cube and homogeneous Dirichlet conditions are imposed on the rest of the faces. The solution is advanced up to time 0.1. To the right in Figure 2 the difference in discrete energy between subsequent time steps is plotted. As can be seen the size of the difference is at machine precision, thus verifying the correctness of the implementation and the conservation properties of the method.

4.3 Effects of curvature in a thin wave guide

It is known that the properties of surface waves in solids depend on both the curvature and the polarization of the displacement field [3]. For certain polarizations and curvature the group and / or phase velocities of the surface waves increase and for other they decrease. These features can be used in nondestructive testing applications to, for example, determine the effect of change in cross section of free surface wave-guides, see [16].

In this example we consider a problem setup, inspired by the experiments in [16], consisting of a thin long aluminum wave guide with a slowly varying cross section, see Figure 3. The material properties of the wave guide are given by $\lambda=70GPa$, $\mu=35GPa$,

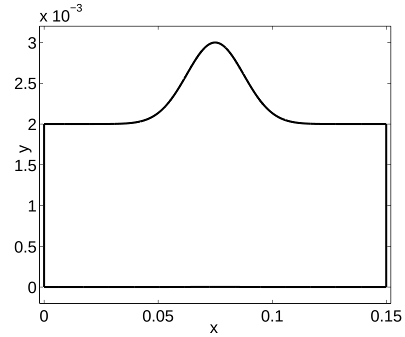

Figure 3: The thin wave guide with a small perturbation on the upper side. Note that the scaling of the axis are very different. The units of the axis are given in meter.

$\rho = 2700 kg/m^3$. The guide is 150 mm long and at the ends it is 2 mm wide. The upper surface of the wave guide is described by the equation

$$y(x) = 2 + e^{-0.003203(x-75)^2},$$

where x and y are given in mm. The rightmost part of the wave guide is clamped and the other three sides are free.

We are interested in how small wave packages, mainly confined to the free surface, are affected by the curvature. To create such wave packages we add a time dependent forcing to the free surface boundary conditions on the boundary to the left. Precisely we take the boundary conditions to be

$$\begin{bmatrix} (2\mu+\lambda)u_x + \lambda v_y & \mu(v_x+u_y) \\ \mu(v_x+u_y) & (2\mu+\lambda)v_y + \lambda u_x \end{bmatrix} \begin{bmatrix} \bar{q}_x \\ \bar{q}_y \end{bmatrix} = \begin{bmatrix} 0 \\ 5\cdot 10^8 g(t) \end{bmatrix} \tag{4.3}$$

were

$$g(t) = \sin(2\pi f t) e^{-\left(\frac{t-t_0}{\delta}\right)^2},$$
$$f = 5.0 MHz,\ \ t_0 = 2\mu s,\ \delta = 0.5\mu s.$$

The wave-guide is discretized using a grid consisting of 7502×103 points. Towards the ends of the grid each cell is approximately a square with side $\sim 20\mu m$ while at the bump the cells are slightly rectangular with a shortest side in the x direction of $20\mu m$. For the waves induced by the boundary condition (4.3) this discretization gives a resolution of approximately 20 points per wavelength.

The simulation runs up to time $t = 35\mu s$ and the solution is saved at some different time instants. In Figure 4 an overlay contour plot of the magnitude of the solution at times $t = 15.9\mu s$, $23.8\mu s$, $31.8\mu s$ is shown. Initially the wave packages travel with the same speed but as the wave guide expands, the wave package along the curved boundary

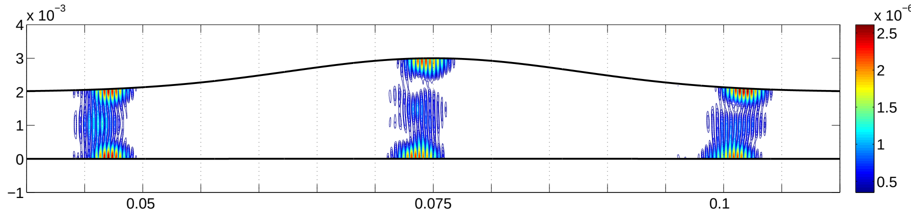

Figure 4: Magnitude of the solution at three time instants, $t=15.9\mu s$, $23.8\mu s$, $31.8\mu s$. The upper wave package is accelerated as it passes the curved section and arrives first to the clamped boundary to the right.

accelerates and moves ahead of the package at the flat boundary, see also Figure 5 for a close up of the magnitude of the solution along the boundaries.

This experiment illustrates that, even for small changes in curvature, accurate representation of the geometry is crucial to obtain the correct results.

4.4 Effects of topography in two dimensions

Curved surfaces, or rather topography, can have significant effects on the ground motions after a seismic event. To illustrate this we solve a variation of Lamb's problem on a domain with a simple topographical feature. The computational domain is composed of a "halfspace" $x\in[-20,20]$ km and $y\in[0,-20]$ km. In the left part of the halfspace there is a small mountain whose elevation (in kilometers) is described by the equation

$$y(x)=0.2\exp\left(-\left(\frac{x-15.0}{0.3}\right)^2\right).$$

To separate the effect of curvature from effects from material heterogeneity the halfspace is assumed to be homogeneous with P-wave velocity $C_p=3.2$ km/s, S-wave velocity $C_s=1.8475$ km/s and density $\rho=2200.0$ kg/m^3.

At time zero the displacements and velocities are zero and the problem is forced by adding the following source to the free surface at the top of the domain

$$\left[\begin{array}{cc}(2\mu+\lambda)u_x+\lambda v_y & \mu(v_x+u_y)\\ \mu(v_x+u_y) & (2\mu+\lambda)v_y+\lambda u_x\end{array}\right]\left[\begin{array}{c}\bar{r}_x\\ \bar{r}_y\end{array}\right]=\delta(x)\delta(y)g(t)\left[\begin{array}{c}\bar{r}_x\\ \bar{r}_y\end{array}\right],$$

were the time dependence is given by a Ricker wavelet

$$g(t)=10^{13}\,(2(\pi f_0(t-t_0))^2-1)e^{-(\pi f_0(t-t_0))^2},$$

and $t_0=1s$ and $f_0=2$ Hz. The domain is discretized with 2001×1001 points and the solution is advanced using a time step $k=0.004329s$ for ten seconds. The results of the simulations can be found in Figure 6. The small mountain in the left part of the halfspace acts as a scatterer, creating a new family of backscattered P, S and Rayleigh waves. The amplitude of the reflected Rayleigh wave is quite substantial and clearly illustrates the important effect of topography.

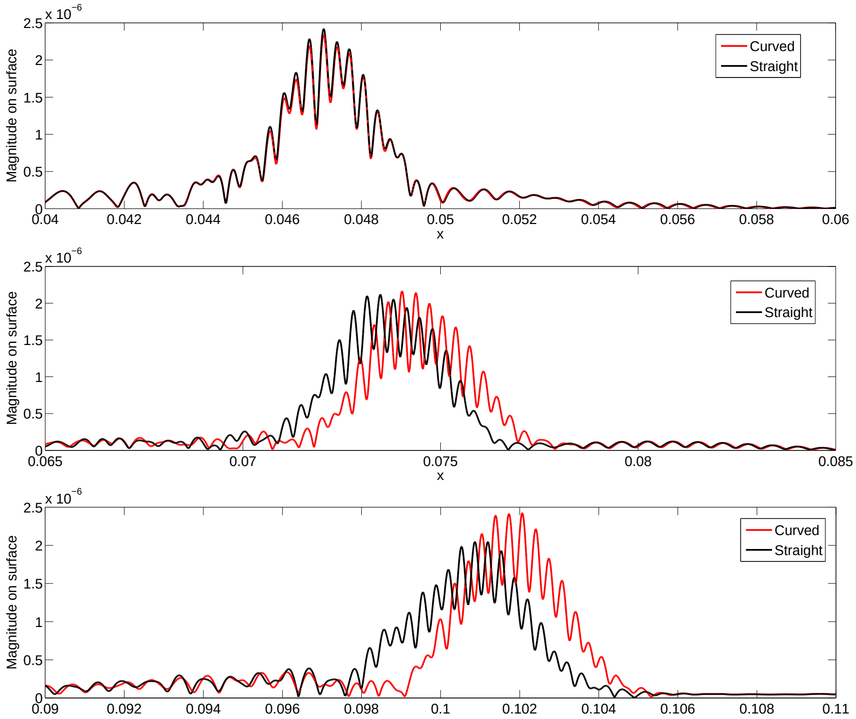

Figure 5: From top to bottom: Magnitude of the solution at time $15.9\mu s$, $23.8\mu s$ and $31.8\mu s$. Note that the start and of the horizontal axis are different in the different plots.

4.5 Effects of topography in three dimensions

As a first three dimensional problem we consider an example from [13] ("amplification of a three-dimensional hill") with a three dimensional topography. The topography is described by the hill

$$z(x,y) = 180\exp\left(-\left(\frac{x-1040}{500}\right)^2 - \left(\frac{y-1040}{250}\right)^2\right) m, \quad (x,y) \in [0m, 2080m]^2.$$

The computational domain extends to the depth $z(x,y) = -1050m$. The medium is homogeneous with $V_p = 3200m/s$, $V_s = 1847.5m/s$ and $\rho = 2200\text{kg}/m^{-3}$. At the bottom u,v and w prescribed according to:

$$u(x,y,-1050) = 0, \quad v(x,y,-1050) = 0,$$
$$w(x,y,-1050) = 0.5(2(10.2\pi(t-0.5))^2 - 1)e^{-(10.2\pi(t-0.5))^2}.$$

At the top surface a free surface boundary condition is imposed and at the other boundaries periodic conditions are imposed.

As in [13] the displacements are measured at the surface along the minor axis (in the y direction). The domain is discretized with 602 grid points in the q and r directions

(a) Magnitude at time 2.5974s

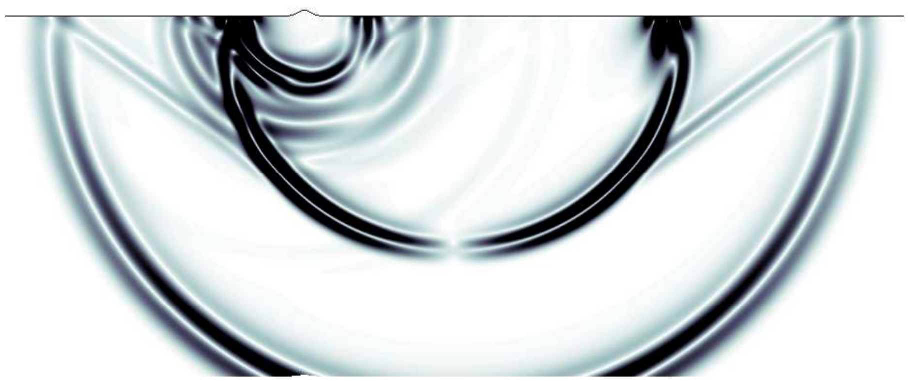

(b) Magnitude at time 5.1948s

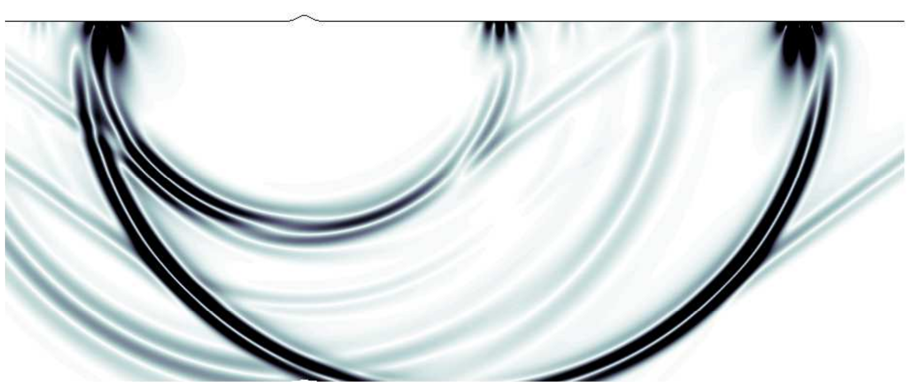

(c) Magnitude at time 7.7922s

Figure 6: Magnitude of the solution at different time instants for the variation of Lamb's problem described in §4.4. The color scale is the same in all of the three frames. The small mountain on the left side of the free surface acts as a scatterer, creating a new family of backscattered P,S and Rayleigh waves.

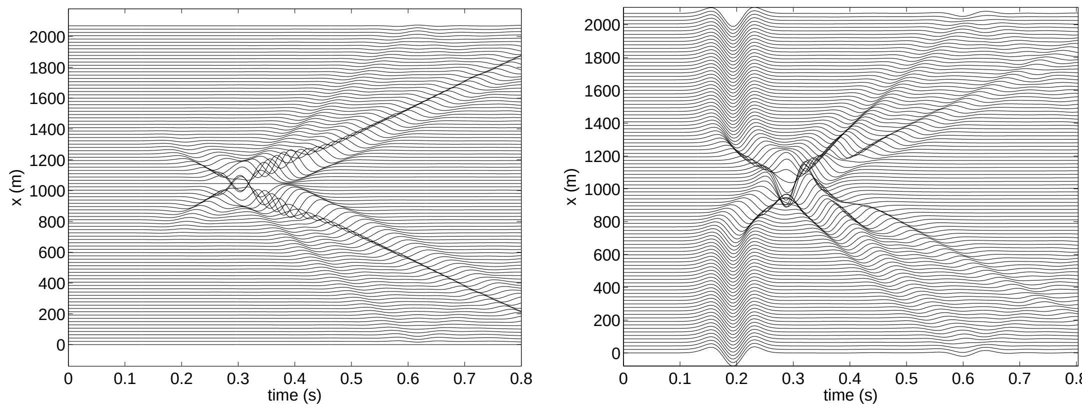

(a) v along the y-axis. (b) w along the y-axis.

Figure 7: Time responses of the v and w components.

and with 303 points in the s direction. In Figure 7 the time responses of the v and w components are found. As can be seen they agree well with the results depicted in Figure 12 in [13].

4.6 Wave propagation in a thin toroidal shell

As a final example we consider the propagation of waves in a thin toroidal shell with free surfaces. The toroidal shell is described by the mapping

$$\begin{aligned} x(q,r,s) &= (R_1+(R_2+s\Delta_R)\cos(2\pi r))\cos(2\pi q),\\ y(q,r,s) &= (R_1+(R_2+s\Delta_R)\cos(2\pi r))\sin(2\pi q),\\ z(q,r,s) &= (R_2+s\Delta_R)\sin(2\pi r), \end{aligned} \tag{4.4}$$

where the larger radius is $R_1=4$, the smaller radius is $R_2=1$ and the width of the shell is $\Delta_R=0.1$. The shell consists of a (non-dimensionalized) homogeneous material with $\mu=1$, $\lambda=14$ and density $\rho=1$, i.e. $C_p=4$ and $C_s=1$.

At time zero the shell is at rest and to induce waves we introduce a forcing in the free surface boundary condition at the interior shell. That is, at $s=0$, we impose the boundary condition

$$\begin{bmatrix} (2\mu+\lambda)u_x+\lambda(v_y+w_z) & \mu(v_x+u_y) & \mu(w_x+u_z) \\ \mu(v_x+u_y) & (2\mu+\lambda)v_y+\lambda(u_x+w_z) & \mu(w_y+v_z) \\ \mu(w_x+u_z) & \mu(w_y+v_z) & (2\mu+\lambda)w_z+\lambda(u_x+v_y) \end{bmatrix} \begin{bmatrix} \bar{s}_x \\ \bar{s}_y \\ \bar{s}_z \end{bmatrix} = \begin{bmatrix} f \\ 0 \\ 0 \end{bmatrix}, \tag{4.5}$$

were a point force is applied with a Ricker wavelet time dependence, according to,

$$f = \delta(x-x_0)\delta(y)\delta(z) \times 10000(2(4\pi(t-1))^2 - 1)e^{-(4\pi(t-1))^2},$$

and $x_0 = R_1 + R_2$. Note that the above boundary conditions are stated in Cartesian coordinates (for brevity), in the code we obviously discretize the curvilinear version of (4.5).

Since the shell is very thin compared to its circumference it is a fairly challenging task to solve this problem. To get a grid with reasonably uniform cells the shell is discretized with 5081 points in the q-direction, 1315 points in the r-direction and 21 points in the s-direction. Including ghost points, the total number of grid points amount to about 154 million. With this discretization the solution is advanced up to time 20 using a time step $k = 0.0008135$. At various times, snapshots of the solution on the upper half ($r \in [0,0.5]$) of the inner shell are saved. Some of these snapshots can be found in Figure 8. As can be seen already in subfigure (a), there are a lot of waves that bounce between the free surfaces of the thin shell, generating complicated wave patterns. In the middle of the picture there is a set of smaller wavefronts of faster waves, and further to the right there is a stronger more concentrated wave front of slowly moving waves. At time $\sim$8 (subfigure (b)) the wave pattern is dominated by the waves with short wave length, the thin wave to the right has revolved a lap around the shell and is moving to the left. In the next frame (c) the rightmost wave has emerged from the left and is moving to the right. Further to the left, most of waves are concentrated to the outermost part of the shell. Finally, in subfigure (d) the primary wavefront has just focused in the left part of the torus and is now composed of small localized wave crests.

To get a rough understanding of how well the waves are resolved we plot the solution along the line $A-B$ (see Figure 8 (d)). The different components of the displacements are plotted as a functions of the angle in Figure 9 (a). In subfigure (b) a closeup of the displacements close to the most rapidly varying part of the solution are plotted. Each marker represent a grid point and as we can see the waves are fairly well resolved.

5 Summary and discussion

A stable and explicit finite difference method for the elastic wave equation in curvilinear coordinates has been presented. The discretization of the spatial operators in the method has been shown to be selfadjoint for free-surface, Dirichlet and periodic boundary conditions. The fully discrete version of the method has been shown to conserve a discrete energy to machine precision.

As stated in the introduction it would be of great interest to develop a higher order self-adjoint discretization of the elastic wave equation. The possibilities of using summation by parts techniques to extend the present method to such a high order discretization is currently under investigation.

Another minor drawback of the method is due to the fact that the curvilinear formulation of the elastic wave equation contains many more terms then the Cartesian formulation, making the method more expensive than a method on a Cartesian grid. The remedy to this is to use an overlapping grid approach (see e.g. [5]) where the equations close to curved boundaries are solved on body fitted curvilinear grids, the equations in the interior are solved on Cartesian grids and communication between grids are handled via interpolation.

Acknowledgments

Daniel Appelö would like to thank Björn Sjögreen and William Henshaw for stimulating discussions . This work performed under the auspices of the U.S. Department of Energy by Lawrence Livermore National Laboratory under Contract DE-AC52-07NA27344.

A

Expressions for $\mathcal{P}_1,\mathcal{P}_2,\mathcal{P}_3,\mathcal{P}_4$ in Lemma 2.

$$\begin{aligned}\mathcal{P}_1 = &\|\sqrt{J\lambda}(q_x\widetilde{D_0^q}u + r_xD_0^ru + q_y\widetilde{D_0^q}v + r_yD_0^rv)\|_h^2 + \|\sqrt{J2\mu}(q_x\widetilde{D_0^q}u + r_xD_0^ru)\|_h^2\\ &+\|\sqrt{J2\mu}(q_y\widetilde{D_0^q}v + r_yD_0^rv)\|_h^2 + \|\sqrt{J\mu}(q_y\widetilde{D_0^q}u + r_yD_0^ru + q_x\widetilde{D_0^q}v + r_xD_0^rv)\|_h^2,\end{aligned} \tag{A.1}$$

$$\begin{aligned}\mathcal{P}_2 = &\frac{h_r^2}{4}\Big(\|\sqrt{J2\mu}r_xD_+^rD_-^ru\|_h^2 + \|\sqrt{J2\mu}r_yD_+^rD_-^rv\|_h^2\Big)\\ &+\frac{h_q^2}{4}\Big(\|\sqrt{J2\mu}q_xD_+^qD_-^qu\|_{hr}^2 + \|\sqrt{J2\mu}q_yD_+^qD_-^qv\|_{hr}^2\Big)\\ &+\frac{h_r^2}{4}\|\sqrt{J\lambda}(r_xD_+^rD_-^ru + r_yD_+^rD_-^rv)\|_h^2 + \frac{h_q^2}{4}\|\sqrt{J\lambda}(q_xD_+^qD_-^qu + q_yD_+^qD_-^qv)\|_{hr}^2\\ &\frac{h_r^2}{4}\|\sqrt{J\mu}(r_xD_+^rD_-^rv + r_yD_+^rD_-^ru)\|_h^2 + \frac{h_q^2}{4}\|\sqrt{J\mu}(q_xD_+^qD_-^qv + q_yD_+^qD_-^qu)\|_{hr}^2,\end{aligned} \tag{A.2}$$

$$\begin{aligned}\mathcal{P}_3 = \frac{h_r}{2}\sum_{j=1}^{N_r}\Big(&(J\lambda)_{N_q,j}((q_x)_{N_q,j}u_{N_q-1,j} + (q_y)_{N_q,j}v_{N_q-1,j})^2\\ &+(J\mu)_{N_q,j}((q_x)_{N_q,j}v_{N_q-1,j} + (q_y)_{N_q,j}u_{N_q-1,j})^2\Big),\end{aligned} \tag{A.3}$$

$$\mathcal{P}_4 = \frac{h_q h_r}{2}\sum_{j=1}^{N_r}\Big((J\lambda)_{3/2,j}((q_x)_{3/2,j}D_+^q u_{1,j} + (q_y)_{3/2,j}D_+^q v_{1,j})^2 + (J\mu)_{3/2,j}((q_x)_{3/2,j}D_+^q v_{1,j} + (q_y)_{3/2,j}D_+^q u_{1,j})^2 + (J2\mu)_{3/2,j}(((q_x)_{3/2,j}D_+^q u_{1,j})^2 + ((q_y)_{3/2,j}D_+^q v_{1,j})^2)\Big). \quad \text{(A.4)}$$

References

[1] Z. Alterman and F. C. Karal. Propagation of elastic waves in layered media by finite difference methods. *Bulletin of the Seismological Society of America*, 58(1):367–398, 1968.

[2] Z. Alterman and A. Rotenberg. Seismic waves in a quarter plane. *Bulletin of the Seismological Society of America*, 59(1):347–368, 1969.

[3] L.M. Brekhovskikh. Surface waves confined to the curvature of the boundary in solids. *Soviet Physics - Acoustics*, 13(4):462–472, 1968.

[4] D. L. Brown. A note on the numerica solution of the wave equation with piecewise smooth coefficients. *Mathematics of Computations*, 42(166):369–391, 1984.

[5] G. Chesshire and W. Henshaw. Composite overlapping meshes for the solution of partial differential equations. *Journal of Computational Physics*, 90, 1990.

[6] G. C. Cohen. *Higher-Order Numerical Methods for Transient Wave Equations*. Springer, 2002.

[7] E. Faccioli, F. Maggio, R. Paolucci, and A. Quarteroni. 2d and 3d elastic wave propagation by a pseudo-spectral domain decomposition method. *Journal of Seismology*, 1(3):237–251, 1997.

[8] K-A. Feng, C-H. Teng, and M-H. Chen. A pseudospectral penalty scheme for 2d isotropic elastic wave computations. *Journal of Scientific Computing*, 33(3):313–348, 2007.

[9] B. Fornberg. The pseudospectral method: Comparisonswith finite differences for the elastic wave equation. *Geophysics*, 52(4):483–501, 1987.

[10] A. Ilan and D. Loewenthal. Instability of finite difference schemes due to boundary conditions in elastic media. *Geophysical Prospecting*, 24, 1976.

[11] Almoga Ilan. Stability of finite difference schemes for the problem of elastic wave propagation in a quarter plane. *Journal of Computational Physics*, 29, 1978.

[12] M. Käser and M. Dumbser. An arbitrary high-order discontinuous galerkin method for elastic waves on unstructured meshes - i. the two-dimensional isotropic case with external source terms. *Geophysical Journal International*, 166(2):855–877, 2006.

[13] D. Komatitsch and J.-P. Vilotte. The spectral element method; an efficient tool to simulate the seismic response of 2d and 3d geological structures. *Bulletin of the Seismological Society of America*, 88(2):368–392, 1998.

[14] H.-O. Kreiss and J. Oliger. Comparison of accurate methods for the integration of hyperbolic equations. *Tellus*, 24:199–215, 1972.

[15] B. Lombard, J. Piraux, C. Gelis, and J. Virieux. Free and smooth boundaries in 2-d finite-difference schemes for transient elastic waves. *Geophysical Journal International*, XXX(XXX):xxx–xxx, 2007.

[16] P. Marical, M. Ech-Cherif El-Kettani, and M.V. Predoi. Guided waves in elastic plates with gaussian section variation: Experimental and numerical results. *Ultrasonics*, 47(1-4):1–9, 2007.

[17] S. Nilsson, N. A. Petersson, B. Sjögreen, and H.-O. Kreiss. Stable difference approximations for the elastic wave equation in second order formulation. *SIAM Journal on Numerical Analysis*, 45(5):1902–1936, 2007.

[18] Stacey R. New finite-difference methods for free surfaces with a stability analysis. *Bulletin of the Seismological Society of America*, 84(1):171–184, 1994.

[19] J. F. Thompson, Z. U.A. Warsi, and C. W. Mastin. *Numerical grid generation: foundations and applications*. Elsevier North-Holland, Inc., New York, NY, USA, 1985.

[20] J. E. Vidale and R. W. Clayton. A stable free-surface boundary condition for two-dimensional elastic finite-difference wave simulation. *Geophysics*, 51, 1986.

[21] W. Zhang and X. Chen. Traction image method for irregular free surface boundaries in finite difference seismic wave simulation. *Geophysical Journal International*, 167(1):337–353, 2006.

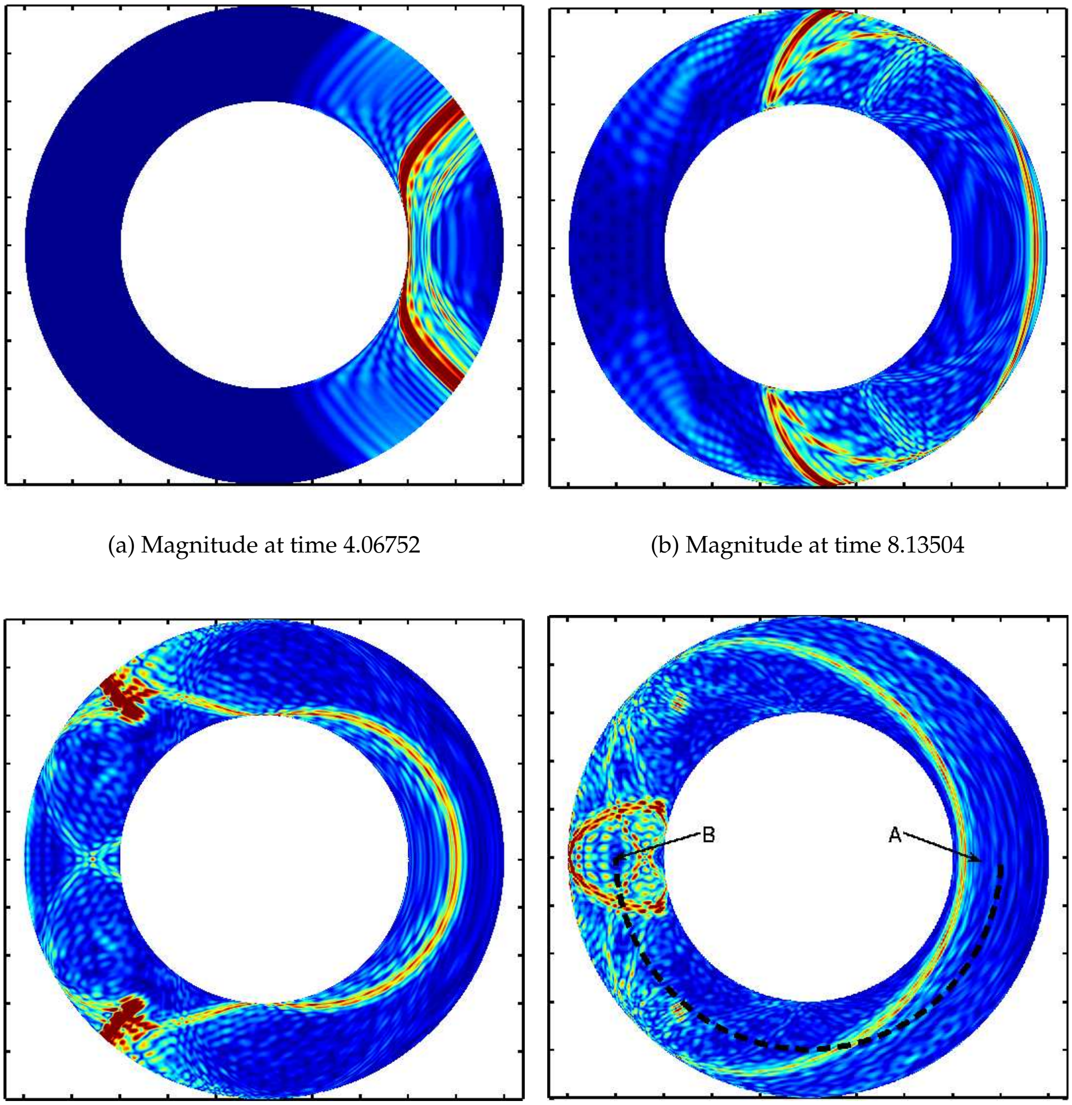

(a) Magnitude at time 4.06752

(b) Magnitude at time 8.13504

(c) Magnitude at time 12.2026

(d) Magnitude at time 16.2701

Figure 8: The magnitude of the wave field at different times on the upper half of the inner surface in the three dimensional toroidal shell described by the mapping (4.4).

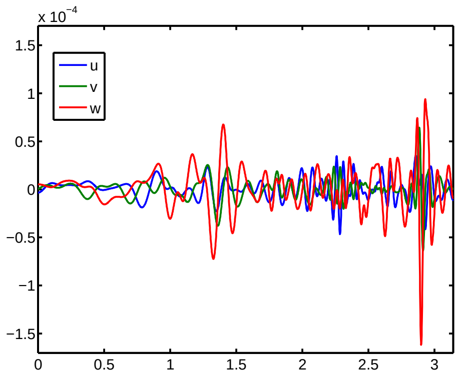

(a) The solution along the centerline $A-B$ (see Figure 8 (d)).

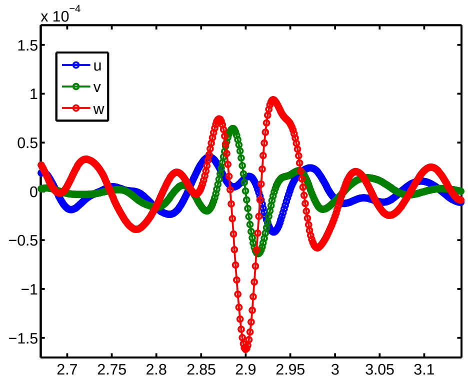

(b) Zoom in on the most osculating part, each marker represent a grid point. Even the steepest waves are fairly well resolved.

Figure 9: The solution along the line $A-B$ (see Figure 8 (d) at time 16.2701